Available online at www.sciencedirect.com

ScienceDirect

Advances in Space Research 72 (2023) 115–128

ADVANCES IN SPACE RESEARCH (a COSPAR publication)

www.elsevier.com/locate/asr

Using DORIS data for validating real-time GNSS ionosphere maps

Ang Liu [a,b], Ningbo Wang [a,b,*], Denise Dettmering [c], Zishen Li [a,b], Michael Schmidt [c], Liang Wang [a], Hong Yuan [a,b]

[a] Aerospace Information Research Institute (AIR), Chinese Academy of Sciences (CAS), 100094 Beijing, China
[b] University of Chinese Academy of Sciences (UCAS), 100049 Beijing, China
[c] Deutsches Geodätisches Forschungsinstitut (DGFI-TUM), Technische Universität München, 80333 München, Germany

Received 26 June 2022; received in revised form 21 December 2022; accepted 23 January 2023
Available online 27 January 2023

Abstract

The ionospheric information retrieved from the Doppler Orbitography and Radiopositioning Integrated by Satellite (DORIS) system provides valuable and external data sources to examine the quality of existing Global Navigation Satellite System (GNSS) generated ionospheric models. The concept of DORIS differential Slant Total Electron Content (dSTEC) analysis is presented, to check the feasibility of DORIS data in the quality assessment of GNSS derived ionosphere models. Thanks to the large relative frequency ratio between the two frequencies of DORIS, the theoretical precision of DORIS dSTEC is at the level of 0.028 TECu, which is about 10 times better than that of GNSS derived dSTEC. Using 48 co-located DORIS beacon sites of the International DORIS service (IDS) and GNSS stations of the International GNSS Service (IGS), the comparison between DORIS and GNSS dSTEC assessments of Real-Time Global Ionospheric Maps (RT-GIMs) from different analysis centers is performed in this paper. The analysis is performed during the first 110 days of 2022. Based on the analysis results of more than 18,000,000 Jason-3 DORIS ionospheric observables, no systematical deviation is found between DORIS and RT-GIM derived dSTECs, with a mean bias of 0.14 TECu. Compared to DORIS dSTEC, the root-mean-square (RMS) of those RT-GIMs reaches 4.5–5.4 TECu at low-latitudes, which is 2.2–3.6 TECu in mid- and high-latitude regions. The latitudinal variation of RT-GIM errors is clearly observed in DORIS dSTEC analysis. In addition, the Pearson correlation coefficient between Jason-3 DORIS dSTEC RMS and GPS-plus-GLONASS dSTEC RMS is 0.81, and no significant dependence on GPS-only or GLONASS-only data is found. It is suggested to perform the dSTEC analysis with higher satellite elevation cutoff angle, e.g., 45°, to ensure a better consistency between DORIS and GNSS dSTEC assessments. Overall, DORIS dSTEC assessment provides an independent reference for the validation of GNSS based ionosphere maps.

Keywords: Real-Time Global Ionospheric Maps (RT-GIM); Doppler Orbitography and Radiopositioning Integrated by Satellite (DORIS); International DORIS Service (IDS); Differential Slant Total Electron Content (dSTEC); External validation

1. Introduction

Within the International GNSS Service (IGS), the high resolution of Global Ionospheric Maps (GIMs) generated in the format of IONosphere map EXchange (IONEX) have been widely used to investigate the Vertical Total Electron Content (VTEC) variation of the Earth's ionosphere (Schaer 1998, Hernández-Pajares et al. 2009). The grid-based ionospheric delay and associated accuracy information (AI) are provided in the IGS GIM, typically with a spatial resolution of 2.5° in latitude and 5° in longitude, respectively (Li et al., 2015, Zhang and Zhao 2018). In addition to rapid and final GIMs accessible with a time latency of few days, several Ionosphere Associate Analysis Centers (IAACs) of the IGS started to provide real-time

* Corresponding author.
E-mail address: wangningbo@aoe.ac.cn (N. Wang).

https://doi.org/10.1016/j.asr.2023.01.050
0273-1177/

GIMs (RT-GIMs) since 2017, including the Chinese Academy of Sciences (CAS, Li et al. 2020), Centre National d'Etudes Spatiales (CNES), Universitat Politècnica de Catalunya (UPC-IonSAT, Yang et al. 2021) and Wuhan University (WHU).

Such RT-GIMs are commonly generated using RT-GNSS data streams from a global network of inhomogeneous GNSS stations provided by the IGS Real-Time Service (IGS-RTS). Instead of providing VTEC information of individual ionospheric grids as defined in the IONEX format, the spherical harmonic expansion up to degrees 15 is presently adopted in both RTCM-SSR (RTCM-SC 2016) and IGS-SSR (IGS 2020) to distribute real-time ionospheric VTEC messages. In case that RT-GIMs are generated by RT-GNSS data but represented mathematically by an approach not based on spherical harmonics, a transformation between the applied approach and the spherical harmonic expansion requires to be performed (Goss et al. 2020a). Erdogan et al. (2021) model VTEC as a series expansion in two-dimensional tensor products of polynomial and trigonometric B-spline functions. The corresponding B-spline series coefficients are estimated from RT-GNSS data and take over the role of the spherical harmonic coefficients. However, in opposite to the latter ones the B-spline coefficients are reflecting VTEC in a small region and not on the global scale and thus, can handle the inhomogeneous distribution of the input data rather efficiently (Erdogan et al. 2020, Goss et al. 2020b). The VTEC correction of a given ionospheric pierce point (IPP) can be computed using the received spherical harmonic coefficients and converted to the slant TEC (STEC) to account for ionospheric path delay using an ionospheric mapping function (Lyu et al. 2018). Based on the RT-GIMs from CAS, CNES, UPC and WHU, an experimental combined IGS RT-GIM is generated by applying a RT-dSTEC weighting method (Liu et al. 2021). When following RTCM-SSR or IGS-SSR standards to transmit those real-time ionospheric corrections, while the occupied bandwidth is significantly less than that of IONEX-based maps, it comes in turn with certain loss of accuracy information compared to original VTEC maps. As such, it is crucial to conduct a comprehensive and independent quality assessment of RT-GIMs.

The accuracy of RT-GIMs can be assessed by comparison with the existing ionospheric TEC products (e.g., the IGS combined GIM, Roma-Dollase et al. 2017, Liu et al. 2018), the observed TECs and associated derivatives (e.g., the differential STEC, Hernández-Pajares et al. 2017), or the external consistency evaluation (e.g., the altimetry observed VTECs, Azpilicueta and Brunini 2009). The IGS combined GIM is commonly used as the first TEC reference to check the consistency between real-time and post-processed GIMs, considering its good reliability and continuous data coverage. Since the present RT-GIMs are fully generated by ground GNSS observations, only external GNSS stations (i.e., not used in the model generation) should be selected to ensure an independent accuracy assessment of RT-GIMs, when using GNSS derived absolute TECs with bias corrected or relative phase TECs as references (Wang et al. 2016, Ren et al. 2019Liu et al. 2023). Among them, GNSS differential STECs (dSTEC) calculated from dual-frequency GNSS carrier phase measurements, were originally developed for the relative weighting of GIMs from individual IAACs (Hernández-Pajares et al. 2009), and recently used to evaluate the performance of different ionospheric models (Hernández-Pajares et al. 2017, Liu et al.2019, Wang et al. 2021). Aside from the self-consistency validation methods described above, the external consistency analysis is required when a direct and truly external assessment is required for those electron content models of the ionosphere. At present, ionospheric VTEC observables from altimetry satellites are used as reliable external references for validating ionospheric models, which shows quantitative consistency with GNSS dSTEC information in collocated analysis scenarios (Hernández-Pajares et al. 2017). It is expected that external ionospheric observables from independent observational sources can contribute to the quality assessment of ionospheric VTEC models.

Indeed, there exists another space-geodetic observation technique, i.e., the Doppler Orbitography and Radiopositioning Integrated by Satellite (DORIS), which provides an external validation of different ionospheric models. While DORIS system is designed for the precise orbit determination based on the principle of Doppler effects (Willis et al. 2007, Auriol and Tourain 2010), the dual-frequency signals of DORIS can also be used to extract ionospheric TEC due to the dispersive nature of the ionosphere (Fleury et al., 1991, Dettmering et al., 2014). In contrast to GNSS stations, which require internet access to distribute observation data, DORIS terrestrial beacons do not need additional communication technique. Hence, it is possible to operate DORIS ground beacons on isolated islands (Dettmering et al. 2014). Compared to other external assessment methods, such as altimetry satellites, DORIS beacon network provides a more uniform coverage of global ionosphere over both continental and oceanic regions, which makes it a reliable data source for external validation of those GNSS derived ionospheric models. As of 2022, DORIS observation data are available from CRYOSAT-2, HY-2C, HY-2D, Jason-3, SARAL, Sentinel-3A, Sentinel-3B and Sentinel-6A satellites, with a time latency of 2–3 days. The near real-time (NRT) DORIS data are available from Jason-3 satellite with a latency of only 2–3 h. Additionally, DORIS ground beacon network has been expanded over the past years. By now, there are around 60 beacons in service. The previous DORIS data format, i.e., DORIS v2.2, has low compatibility with GNSS Receiver Independent Exchange Format (RINEX) observations. A new data format of DORIS measurements, i.e., RINEX DORIS 3.0 (IDS, 2006), was designed to expand the use of DORIS technique. The proposed RINEX DORIS format provides satellite-specific rather than station-specific

DORIS measurements, which is an extension of the existing GNSS RINEX format.

While pseudo-range code observations are available from DORIS system, such data is rarely usable for absolute TEC generation due to their large measurement noises of about 1 km (Mercier et al. 2010). In contrast, the high-quality dual-frequency DORIS phase measurements provide a valuable opportunity to examine the Earth's ionosphere, especially given the globally homogeneous distribution of DORIS ground beacons (Wang and Li 2018, Hernández-Pajares et al. 2020). Compared to the dual-frequency GNSS technique (e.g., L1/L2 or L1/L5 signals), the relative frequency ratio between the two frequencies of DORIS reaches to around 5, which is expected to be more sensitive to detect the ionospheric information and less prone to measurement noises (Dettmering et al. 2014). The standardization of DORIS measurements as well as the decreasing time latency in obtaining DORIS data, also provides the possibility to validate RT-GIMs in RT or NRT by combining with other RT ionospheric observables, e.g., derived from RT-GNSS measurements.

The purpose of this paper is to check the feasibility DORIS data in the performance analysis of different RT-GIMs. Using Jason-3 NRT DORIS data from the International DORIS Service (IDS) and GNSS data of the IGS station network, the consistency between DORIS and GNSS assessments of different RT-GIMs is analyzed. The paper is organized as follows. The description of GNSS and DORIS dSTEC assessment methods is presented at first, followed by the comparison and discussion of DORIS and GNSS dSTEC analysis in RT-GIM validations. Summary and conclusions are finally given.

2. GNSS and DORIS dSTEC assessments

Since DORIS pseudo-range code observations exhibit large measurement noises, only DORIS phase measurements are used in the analysis. The GNSS dSTEC analysis, which is formed by dual-frequency GNSS carrier phase measurements, is described at first. The concept of DORIS dSTEC analysis is then presented, followed by the generation of modeled dSTEC information from RT-GIMs.

2.1. GNSS observed DSTEC

GNSS observed dSTEC is defined as the difference between the given STEC at epoch t along a phase continuous arc and the STEC estimated at its highest satellite elevation, as given in Eq. (1).

$$dSTEC_{GNSS}(t) = \mu \cdot [L_I(t) - L_I(t_{E\max})] \quad (1)$$

in which $t_{E\max}$ corresponds to the epoch of the highest satellite elevation, $L_I(t) = L_1(t) - L_2(t)$ denotes the geometry-free linear combination between carrier phase measurements at the frequencies f_1 and f_2, and the frequency dependent factor μ equals to$1/[40.3 \times 10^{16} \times (f_1^{-2} - f_2^{-2})]$.

As only dual-frequency phase observation data are used in GNSS dSTEC calculation, it avoids the negative effects of amplified pseudorange noises as well as the intra-day variation of receiver biases in carrier-to-code leveling derived TEC observables. Also, GNSS dSTEC analysis gives a direct slant but not vertical assessment of different ionospheric models, which reduces the influence of ionospheric mapping errors on the evaluation result. To present a fair assessment of different RT-GIMs, it is recommended to use observation data of those GNSS stations, which do not used in the RT-GIM generation. However, this is difficult to guarantee in practice, because such RT-GNSS stations used by individual analysis centers are commonly not disclosed.

2.2. DORIS observed dSTEC

In the performance assessment of those RT-GIMs, the following points require to be considered: 1) The selected ionospheric observables should be accessed in real-time (RT) or near-real-time (NRT), because the performance analysis is the first step and the generation of RT or NRT combined GIM is the following target. 2) Since the presently RT-GIMs are generated using ground real-time GNSS stations, especially RT-GNSS streams provided by the IGS-RTS, it would be good if the selected ionospheric observable references are fully intendent to ground GNSS stations. Currently, DORIS provides near real-time observation data, which is one of the ionospheric detection methods with the least time delay except for GNSS observations. And its ionospheric observation is completely independent with GNSS observations. Referring to existing GNSS analysis methods, we extend the GNSS-dSTEC concept to DORIS-dSTEC to validate the accuracy of ionospheric products.

The calculation of DORIS dSTEC is very similar to that of GNSS dSTEC, which is generated based on the dual-frequency DORIS carrier phase measurements, provided in RINEX DORIS format, along the individual phase continuous arc. The illustration of GNSS observed dSTEC, RT-GIM modeled dSTEC and Jason-3 DORIS dSTEC is shown in Fig. 1. GNSS and DORIS dSTEC observables contain ionospheric information to the height of Medium Earth Orbit (MEO) and Low Earth Orbit (LEO), respectively. For Jason-3 satellite, the observed DORIS dSTEC is obtained up to the height of around 1300 km, which contains the full ionosphere and the most contribution of plasmaspheric electron contents (PEC). The influence of the remaining small part of PECs is not considered in DORIS dSTEC assessment, but such systematic errors should be kept in mind when comparing DORIS and GNSS derived analysis results (Azpilicueta and Brunini 2009, Hernández-Pajares et al. 2017).

It is known that the transmitting of dual-frequency DORIS signals refers to different antenna phase centers. Such geometry corrections require to be accounted for in

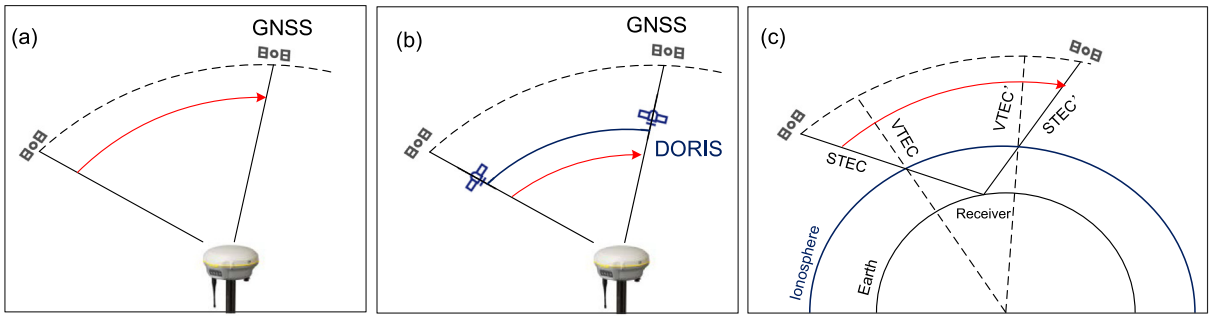

Fig. 1. Illustration of GNSS observed dSTEC(a), DORIS observed dSTEC (b) and RT-GIM derived dSTEC (c).

the extraction of DORIS dSTEC information, as shown below.

$$dSTEC_{DORIS}(t) = \mu[L_I(t) - L_I(t_{E\max}) - (\Delta D(t) - \Delta D(t_{E\max}))] \tag{2}$$

where $\Delta D = D1 - D2$ denotes the associated geometry correction. The distance from DORIS antenna mechanical reference point (antenna base plate) to DORIS MV22 antenna phase center is [2.4128 m, −0.1325 m, 0.555 m] for the first frequency, i.e., 2 GHz, and [2.4128 m, −0.1325 m, 0.9235 m] for the second frequency, i.e., 400 MHz, respectively. The corresponding geometry correction D^s used in Jason-3 DORIS dSTEC extraction is 0.168 m (IDS, 2021). An antenna dependent ground station correction is also required when computing the overall geometry correction, as given in Eq. (5).

$$\Delta D \approx -(D^s + D_b)\sin e \tag{3}$$

using the notation e for satellite elevation angle, $D_b = 0.487$ m for Starec antenna correction, and $D_b = 0.175m$ for former Alcatel antenna correction, respectively.

DORIS phase measurement does not contain any systematic contribution from intentional offsets of transmitter or receiver oscillators. Assuming that the observation noises are $\sigma_{L_1} = 1.5mm$ and $\sigma_{L_2} = 7.5nm$ (i.e., one percent of the wavelength) for DORIS carrier phase measurements at the f_1 and f_2 frequencies, the typical error of DORIS derived dSTEC can be estimated following Eq. (4).

$$\begin{cases} \sigma^2_{dSTEC} = 2\mu^2\sigma^2_{L_I} \\ \sigma^2_{LI} \approx \sigma^2_{L_1} + \sigma^2_{L_2} \end{cases} \tag{4}$$

where σ_{L_I} denotes the precision of geometry-free linear combination of DORIS dual-frequency phase measurements. Clearly, the correlation between L1 and L2 phase measurements is ignored in Eq. (4).

Overall, the theoretical precision reaches 0.028 TECu for DORIS observed dSTEC. The thermal noise of GNSS carrier phase measurements is normally at the level of 2 mm (Li et al. 2020). In this case, the precision of GNSS derived dSTEC is around 0.26 TECu. Obviously, DORIS dSTEC presents significant higher theoretical precision than that of GNSS dSTEC. If we further simplify Eq. (4) by estimating the partial derivative of dSTEC with respect to the frequency differences between f_1 and f_2, we can obtain

$$\frac{\delta\sigma_{dSTEC}}{\delta\Delta} = -\frac{8f_2^4\mu\sigma^2_{L_I}(\Delta + f_2)}{40.3(\Delta^2 + 2f_2\Delta)} < 0 \tag{5}$$

where $\Delta = f_1 - f_2$ denotes the difference between two frequencies f_1 and f_2. This partial differential equation shows that, the precision of derived dSTEC would benefit from a larger frequency difference. Since the frequency difference of DORIS ($\Delta_{DORIS} = 1600MHz$) is much larger than that of GNSS ($\Delta_{GNSS(L1.L2)} = 347.82MHz$), it is expected that the precision of dSTEC extracted by DORIS would be better than that of GNSS. The theoretical precision of DORIS dSTEC is about 10 times better than GNSS dSTEC. Such ultra-precise DORIS dSTEC observables should significantly benefit the quality assessment of different RT-GIMs.

2.3. RT-GIM derived dSTEC

RT-GIM generated dSTEC (i.e.,$dSTEC_{RTGIM}$) of the same epoch and location with respect to GNSS or DORIS derived dSTECs can be calculated as

$$\begin{aligned} dSTEC_{RTGIM}(t) = {} & VTEC_{RTGIM}(\beta,\lambda,t)\cdot MF(e) \\ & - VTEC_{RTGIM}(\beta_{E\max},\lambda_{E\max},t_{E\max})\cdot MF(e_{E\max}) \end{aligned} \tag{6}$$

with the notation β and λ for the geographic latitude and longitude of the ionospheric pierce point (IPP), t for the calculation epoch, e for the satellite elevation angle,$VTEC_{RTGIM}$ for RT-GIM generated VTEC, and $MF(t)$ for the ionospheric mapping function (MF) to convert the estimated VTEC to the line-of-sight STEC.

Note that RT-GIM is not provided in the IONEX format, but spherical harmonic expansion coefficients defined in RTCM-SSR and IGS-SSR standards. The calculation of RT-GIM derived VTEC is given as follows.

$$VTEC_{RTGIM}(\beta,\lambda,t)=\sum_{n=0}^{n_{\max}}\sum_{m=0}^{\min(n,m_{\max})}\tilde{P}_{nm}(\sin\beta)\times\left(\tilde{A}_{nm}(t)\cos(m\lambda)+\tilde{B}_{nm}(t)\sin(m\lambda)\right) \tag{7}$$

where $\tilde{P}_{nm}$ is the normalized associated Legendre function with the degree n and order$m$,$\tilde{A}_{nm}$ and $\tilde{B}_{nm}$ are the spherical harmonic coefficients of associated RT-GIMs.

GNSS and DORIS dSTEC assessments are performed by analyzing the differences between GNSS/DORIS observed dSTEC and RT-GIM derived dSTEC of the same time and location. Referring to Hernández-Pajares (2017), the generated dSTEC residuals are then used to calculate different statistics, e.g., the bias, standard deviation (STD), and root mean square (RMS), for further analysis, shown as follow:

$$\begin{cases} BIAS=\dfrac{\sum_{n=1}^{N}\left(dSTEC_{RTGIM}-dSTEC_{ref}\right)}{N} \\ STD=\sqrt{\dfrac{\sum_{n=1}^{N}\left(dSTEC_{RTGIM}-dSTEC_{ref}-BIAS\right)^2}{N-1}} \\ RMS=\sqrt{\dfrac{\sum_{n=1}^{N}\left(dSTEC_{RTGIM}-dSTEC_{ref}\right)^2}{N}} \end{cases} \tag{8}$$

in which N is the number of validation samples, and $dSTEC_{ref}$ is the dSTEC information which are set as the validation reference, i.e., $dSTEC_{GNSS}$ and $dSTEC_{DORIS}$ in this work. The statistic of BIAS is used to analyze the systematic deviation between RT-GIM and DORIS derived ionospheric observables. STD shows the stability of the ionospheric residuals while ignoring the bias. RMS is used to check the overall precision of different RT-GIM. The three indexes are comprehensively used to quantitatively evaluate the performance of different RT-GIMs.

3. Data sets

Using NRT DORIS data from Jason-3 and GNSS data of the IGS stations, the quality of RT-GIMs from different IAACs are evaluated. To check the consistency of DORIS and GNSS dSTEC assessments in the analysis of different RT-GIMs, 48 co-located DORIS sites of the IDS and GNSS stations of the IGS are selected, as shown in Fig. 2. GPS and GLONASS phase measurements with a sampling rate of 30 s are used to generate GNSS dSTEC observables. The detection of gross errors and cycle slips are applied in the process of GNSS dSTEC extraction.

For DORIS dSTEC, it is retrieved from Jason-3 NRT DORIS measurements, whose interval is 10 s with one intermediate measurement shifted by 3 s. As of 2022, DORIS NRT data are only available from Jason-3, provided in the format of RINEX DORIS 3.0 with a latency of 2–3 h. The NRT orbits computed by the on-board DORIS Navigator (DIODE) of Jason-3 is distributed by CNES in Standard Product-3 (SP3) format, with the same time latency to NRT DORIS measurements. In DORIS dSTEC computation, the observation arcs that contain epochs less than a defined minimum number of 100 are omitted. The geometry-free linear combination of DORIS L1/L2 phase measurements is formed to check the potential large jumps or cycle slips in phase measurements. The difference of phase geometry-free combinations between consecutive epochs are checked, by comparing to the predefined threshold of 0.5 TECu. The satellite cut-off elevation is set to 15° in both GNSS and DORIS dSTEC analysis.

As an example, the distribution of ionospheric observables derived from the co-located Jason-3 DORIS beacons and GNSS stations is also shown in Fig. 2. The ionospheric observables are presented during UTC 00:00–02:00 on DOY 098, where DORIS and GNSS based IPPs are given in green and yellow dots, respectively. Although only GPS and GLONASS data are used in the extraction of GNSS ionospheric observables, GNSS based ionospheric pierce points notably exceed those generated by DORIS, because the NRT DORIS data are only available from Jason-3 by now.

The test time span covers the first 110 days of 2022, i.e., from January 1 to April 20. RT-GIMs from CAS, CNES, UPC, WHU as well as the IGS RT-combined one are included in the analysis, which are abbreviated as RT-CAS, RT-CNES, RT-UPC, RT-WHU, and RT-IGS, respectively, in subsequent sections. Time series of solar flus index F10.7 and geomagnetic index Dst are plotted in Fig. 3. The averaged F10.7 index reaches 109.8 solar flux units (sfu) during the analysis period, with a sharp increase on the day of year (DOY) 090. For the Dst index, it is generally considered that a small geomagnetic storm occurs when Dst index is less than −30 nanoTesla (nT). This threshold is represented by a green line in the bottom panel of Fig. 3. The notably increased solar conditions and geomagnetic storms will affect the performance of different RT-GIMs.

4. Results and discussion

In this section, the quality assessment of different RT-GIMs with respect to DORIS observed dSTEC is presented at first. The comparison between DORIS and GNSS dSTEC assessments is then checked.

4.1. DORIS dSTEC assessment

The comparison between Jason-3 DORIS observed dSTEC and CAS RT-GIM modelled dSTEC is presented in Fig. 4 for DOY 098, 2022. DORIS dSTEC observables are derived by the selected DORIS beacons as shown in Fig. 2. The mean bias between observed and modeled dSTEC is 0.01 TECu, and the associated STD is 0.72 TECu. A good agreement is seen in DORIS observed dSTEC and RT-GIM derived dSTEC series. Such result

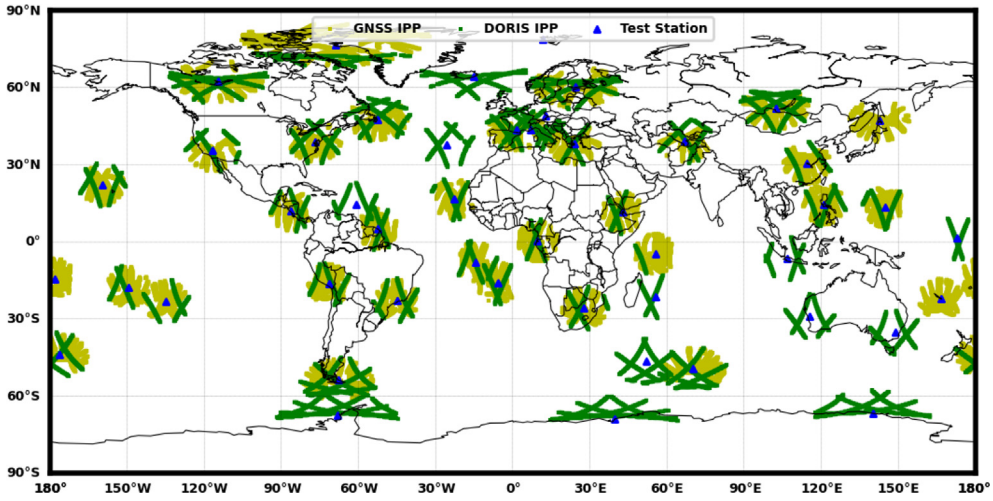

Fig. 2. The selected 48 DORIS beacons and co-located GNSS stations (blue triangle). DORIS and GNSS based ionospheric pierce points are given in green and yellow dots, respectively, during UTC 00:00–02:00 of DOY 098, 2022.

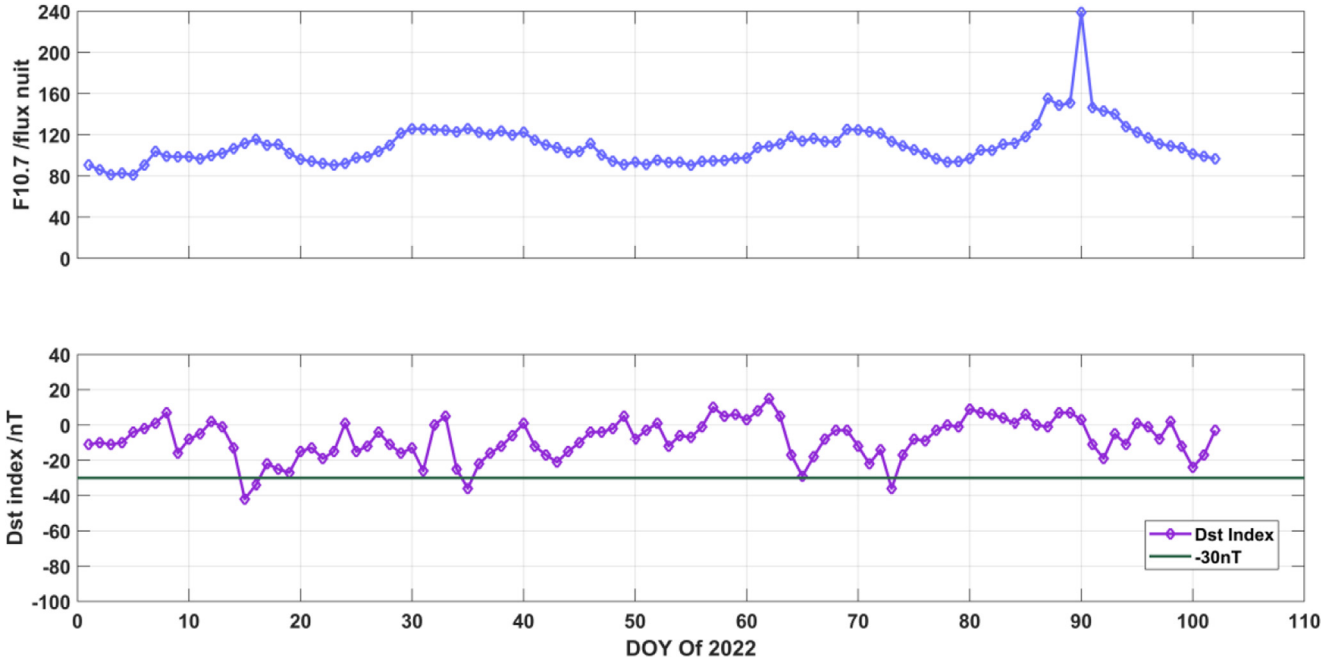

Fig. 3. Time series of F10.7 solar flux (top) and Dst index (bottom) during the test period.

gives an initial proof of using DORIS data for validating the performance of different RT-GIMs.

The latitudinal variation of different RT-GIMs with respect to DORIS dSTEC is evaluated on the same day (DOY 098), by analysing the bias and STD of individual RT-GIMs at the selected 48 DORIS beacons. Fig. 5 shows the bias and STD of RT-GIMs from CAS, CNES, UPC, WHU and IGS at each DORIS beacon station. It is found that the mean difference between individual RT-GIM and referenced DORIS dSTEC is around zero at each DORIS station. As expected, the consistency between RT-GIM derived dSTEC and DORIS observed dSTEC is much better at mid- and high-latitude stations than that of low latitude stations. The influence of the equatorial anomaly on the analysis result can be clearly seen, with the maximum STD values appearing at the equatorial region and minimum values at mid-latitudes of the southern and northern hemispheres.

Fig. 6 shows the distribution of differences between RT-GIM derived dSTECs of all IAACs and dSTEC references generated by Jason-3 DORIS data covering the whole test period. More than 18,000,000 DORIS dSTEC observables are included in the analysis. Compared to DORIS observed dSTEC, the mean bias is 0.14 TECu for RT-GIM derived dSTEC. Around 77.1 % of the dSTEC differences is below +/- 3.0 TECu, and the obtained STD is 4.38 TECu.

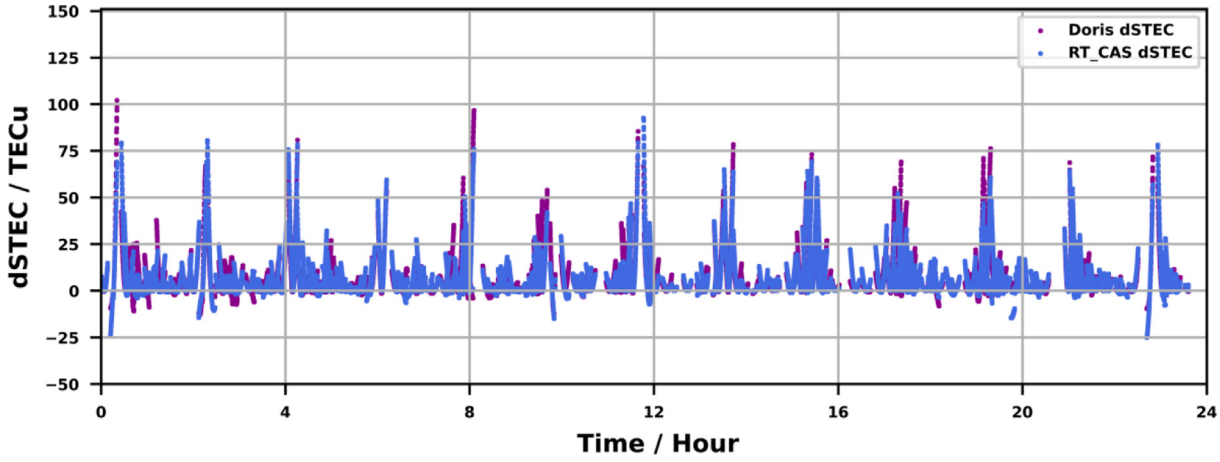

Fig. 4. Jason-3 DORIS observed dSTEC and CAS RT-GIM modelled dSTEC for DOY 098, 2022.

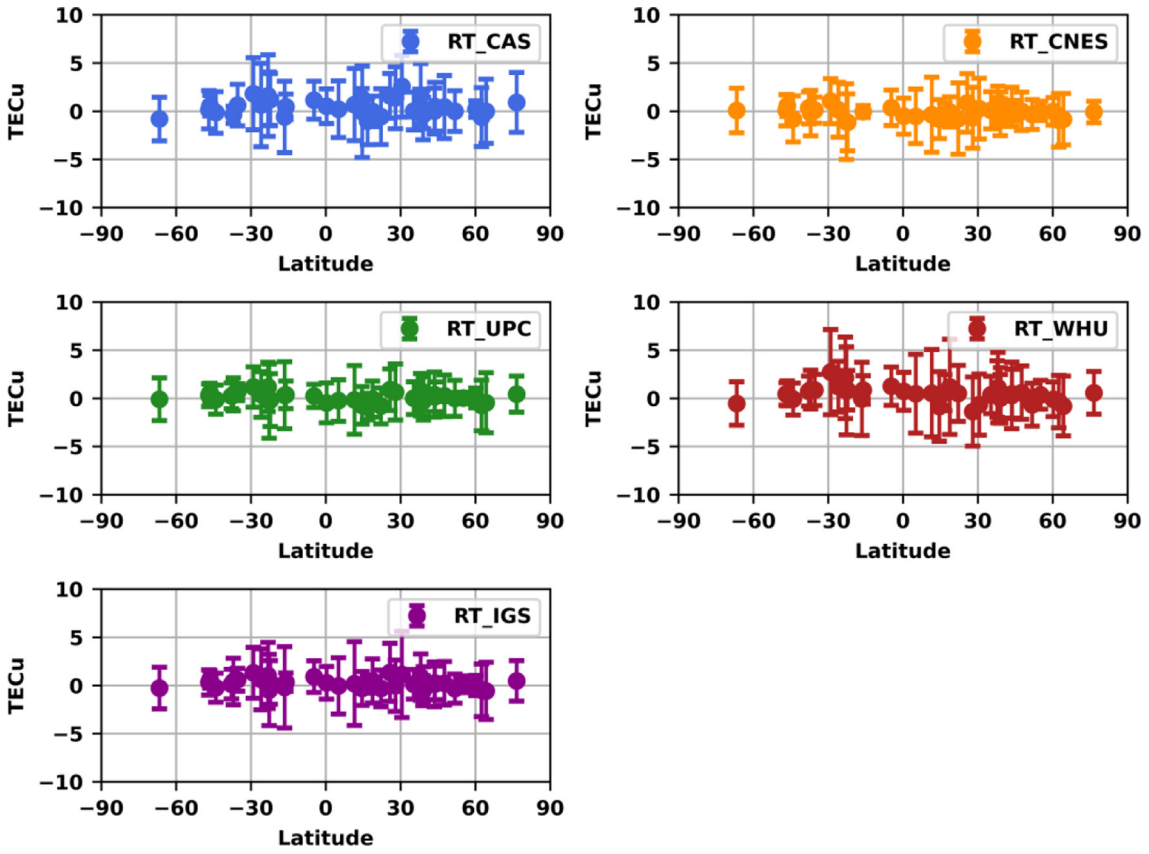

Fig. 5. Error bar of bias and STD of different RT-GIMs compared to observed dSTEC at individual DORIS beacons on DOY 098, 2022. The mean differences are plotted together with their standard deviations at each station, where the center dot and error bar denote the mean bias and STD, respectively.

Clearly, no significant systematic bias is found between Jason-3 DORIS observed dSTEC and RT-GIM derived dSTEC.

To analyze the day-to-day performance variation of different RT-GIMs, the daily bias and STD of dSTEC differences between RT-GIMs from CAS, CNES, UPC, WHU, IGS and Jason-3 DORIS observed dSTECs are calculated and plotted in Fig. 7. RT-GIM from CNES shows significant negative deviation compared to DORIS dSTEC, which indicates that CNES's RT-GIM underestimates the ionospheric dSTEC observables. In the analysis of STD series, the STD mainly changes within the range of 2.5–8.5 TECu and 3.0–8.8 TECu for RT-GIMs from CNES and WHU, respectively, which are notably larger than the result of CAS, UPC and the IGS combined one. Compared to Jason-3 DORIS dSTEC, the mean biases of differ-

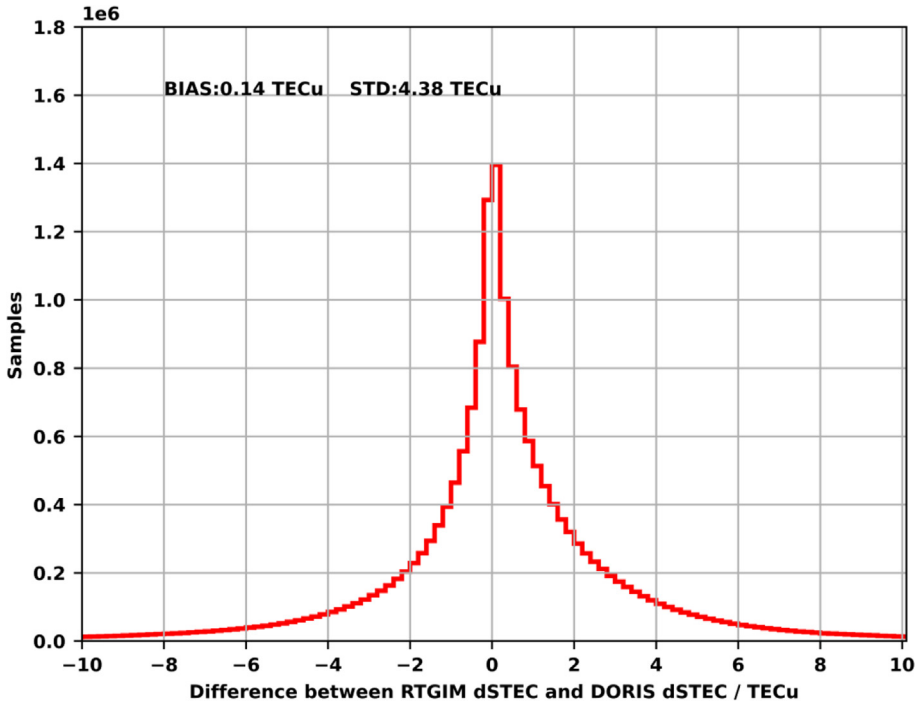

Fig. 6. Histogram of differences between RT-GIM derived dSTECs of all IAACs and Jason-3 DORIS dSTEC observables during DOY 001–110, 2022.

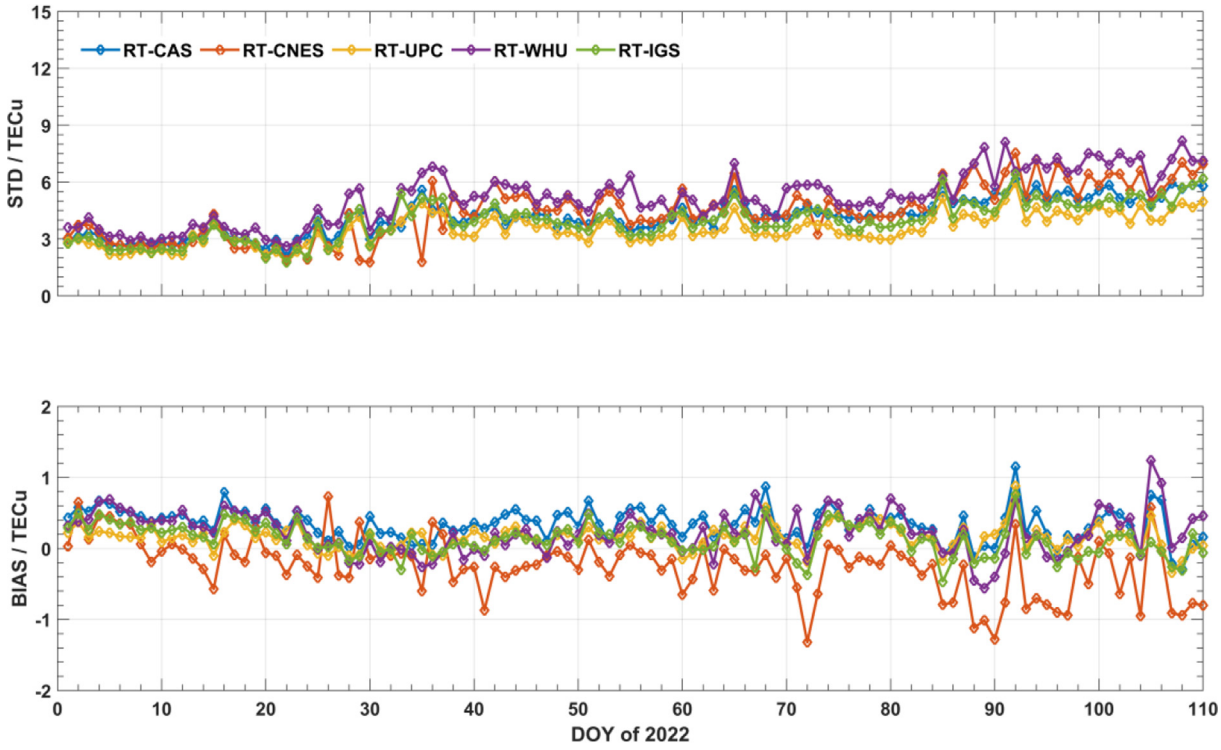

Fig. 7. Bias and STD series of different RT-GIMs compared to Jason-3 DORIS dSTEC.

ent RT-GIMs are 0.37, −0.24, 0.17, 0.32, and 0.15 TECu for CAS, CNES, UPC, WHU and IGS, respectively, with no significant systematic errors. For the STD result, it is 4.21 TECu for CAS, 4.71 TECu for CNES, 3.67 TECu for UPC, 5.46 TECu for WHU and 4.17 TECu for IGS, respectively.

Similar to the day-to-day analysis of different RT-GIMs in comparison to DORIS dSTEC, the daily bias and STD

of individual RT-GIMs compared to GNSS dSTEC are calculated and plotted in Fig. 8. The precision of RT-GIMs from CAS, UPC and the IGS RT-combined one is obviously better than those from CNES and WHU in GNSS dSTEC assessment, which keeps in good accordance with the DORIS dSTEC based analysis. The STD of RT-GIMs from the first three analysis centers is 2–8 TECu, which increases to 4–14 TECu for the last two analysis centers. RT-GIM from CNES still exhibits the largest negative deviation in GNSS dSTEC assessment, whose bias varies between −2.0 and 0.4 TECu. Clearly, UPC's RT-GIM exhibits the best performance in both DORIS and GNSS dSTEC assessments. RT-GIMs from CAS and the IGS RT-combined one perform at a comparable level, which outperforms those RT-GIMs from CNES and WHU during the test period.

When comparing the analysis results presented in Figs. 7 and 8, the STD statistic is higher for GNSS dSTEC than that for DORIS dSTEC. It indicates that the consistency between RT-GIM derived dSTEC and DORIS observed dSTEC is better than that of GNSS dSTEC, when ignoring the systematic bias caused by the different orbital hights of GNSS and DORIS satellites. Since co-located DORIS beacons and IGS stations are used in the analysis, the smaller STD result can be partly attributed to the higher precision of DORIS dSTEC compared to GNSS dSTEC. Additionally, only Jason-3 DORIS data is used in the assessment, whereas GNSS dSTEC validations are performed using GPS and GLONASS observations. More GNSS observations included in the analysis might also contribute to the larger STD statistic. The influence of solar conditions on DORIS and GNSS dSTEC assessments can also be observed. The largest bias and STD variations are found at the end of the period under investigation, which is more likely related to the sudden increased F10.7 index (i.e., 209.8 sfu) on DOY 090 as shown in Fig. 3. A notable jump in the STD series of DORIS dSTEC assessment can be seen on DOYs 015, 035 and 064, which keeps in proper accordance with the high level of geomagnetic conditions on those days. While the Dst index is less than −30 ns on DOY 072 (see Fig. 3), its effects on the STD analysis cannot be clearly observed.

4.2. Comparison between DORIS and GNSS dSTEC validations

Using the selected 48 co-located DORIS beacon sites and GNSS stations, the latitudinal variation of RT-GIM errors in DORIS and GNSS validations is first analyzed. Take CAS RT-GIM as an example, the bias, STD and RMS at different latitudinal bands in DORIS and GNSS assessments are summarized in Table 1. In both DORIS and GNSS dSTEC analysis, the performance of RT-GIM shows a similar latitudinal variation, which exhibits larger errors in low-latitudes than mid- and high-latitude regions. With DORIS dSTEC as reference, the RMS in low-latitudes is 4.5–5.4 TECu, which is 2.2–3.6 TECu in mid- and high-latitudes. Compared to DORIS validations, the RMS statistic in GNSS dSTEC analysis is slightly larger at low-latitudes, and comparable in mid- and high-latitude regions. Additionally, the hemispheric asymmetry of RT-GIM errors (i.e., larger errors in southern hemisphere than northern hemisphere) can also be clearly seen, which keeps in good accord with previous analysis results (Hernández-Pajares et al. 2017, Li et al. 2020, Yang et al. 2021). It should be pointed that only JASON-3 satellite provides NRT DORIS observation data, while the full GPS and GLONASS constellations are included in the

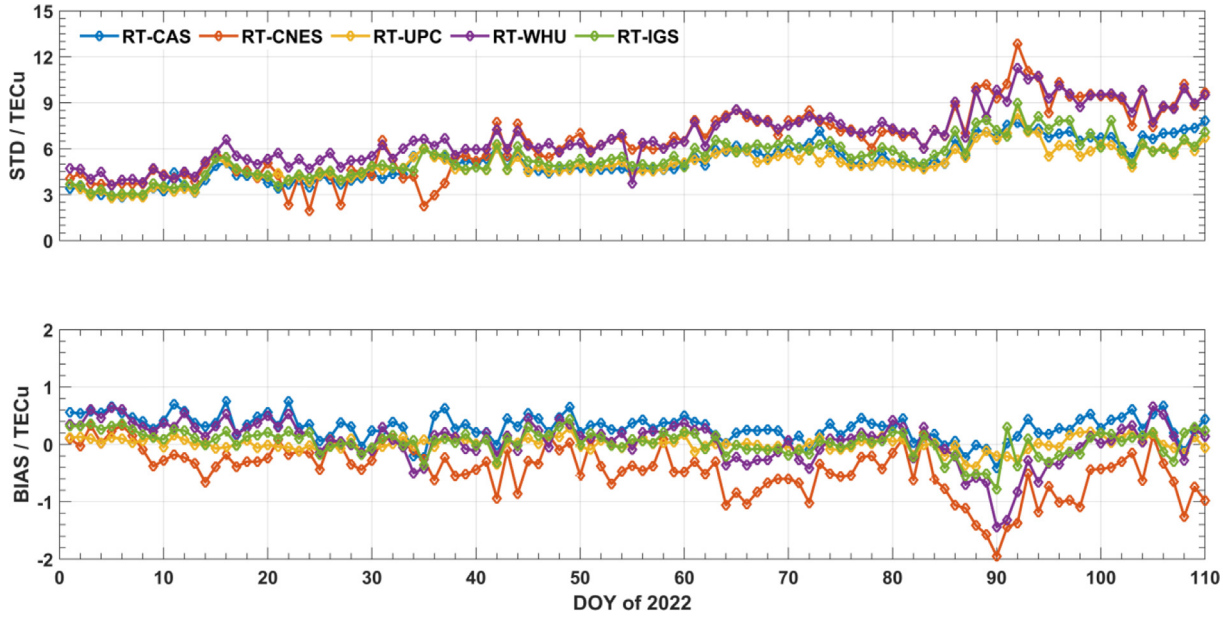

Fig. 8. Bias and STD series of different RT-GIMs compared to GNSS dSTEC.

Table 1
Statistical results of CAS RT-GIMs in DORIS and GNSS dSTEC assessments during DOY 001–110, 2022.

Reference	Index	Latitudinal bands					
		[-90°, −60°]	[-60°, −30°]	[-30°, 0°]	[0°, 30°]	[30°, 60°]	[60°, 90°]
DORIS	Bias	0.14	0.21	0.65	0.44	0.18	0.23
dSTEC	STD	3.53	3.06	4.53	5.30	2.17	2.84
	RMS	3.53	3.06	4.58	5.32	2.18	2.85
GNSS	Bias	−1.17	−0.47	0.62	0.81	−0.10	0.24
dSTEC	STD	3.02	2.64	4.94	5.91	2.22	2.95
	RMS	3.72	2.69	4.97	5.96	2.22	2.96

analysis. As such, the amount of GPS/GLONASS derived dSTEC data are notably larger than those derived by Jason-3 NRT DORIS data. Since the orbital altitude/period of JASON-3 satellite is quite different from GPS and GLONASS satellites, the IPP locations of DORIR and GPS/GLONASS ionospheric observables of the same epoch are not identical for the selected co-located stations. Although the theoretical precision of DORIS-dSTEC is much better than that of GNSS-dSTEC, differences in the distribution of IPPs and number of statistical samples between two validation schemes should notably affect the DORIS assessment results.

With the daily RMS of individual IAACs' RT-GIMs, the correlation coefficient between GNSS dSTEC validation and DORIS dSTEC validation during the test period is provided in Fig. 9. The RMS of RT-GIM dSTEC discrepancy referring to GNSS dSTEC values is larger than that of discrepancy referring to DORIS value, since most values are clearly below the symmetry line (red line). Overall, the Pearson correlation coefficient is 0.81 between DORIS and GNSS dSTEC assessments. We also analyze the correlation between RMS of RT-GIM dSTEC discrepancy referring to DORIS data and RMS of RT-GIM VTEC discrepancy referring to the IGS final GIM, as shown in Fig. 10. In this case, the overall correlation coefficient is 0.71. The validation result using DORIS dSTEC is in general more consistent to the IGS-GIM than using GNSS dSTEC, even though the scatters presented in Fig. 10 are notably larger, especially for RT-GIMs of CNES and WHU. As reported in Hernández-Pajares et al. (2017), the maximum value of the correlation coefficient between GPS dSTEC and Jason-2 VTEC assessments is found to be 0.55 in RMS discrepancy comparison, and 0.78 in relative RMS error comparison. It is confirmed by the correlation analysis of DORIS dSTEC assessment results in comparison to GNSS dSTEC and IGS-GIM VTEC assessments results that, DORIS dSTEC can be used as an independent reference to validate the quality of those GNSS generated ionospheric maps.

Since GPS and GLONASS observation data are used in GNSS dSTEC analysis, we further evaluated the consistency between DORIS and GPS-only as well as DORIS

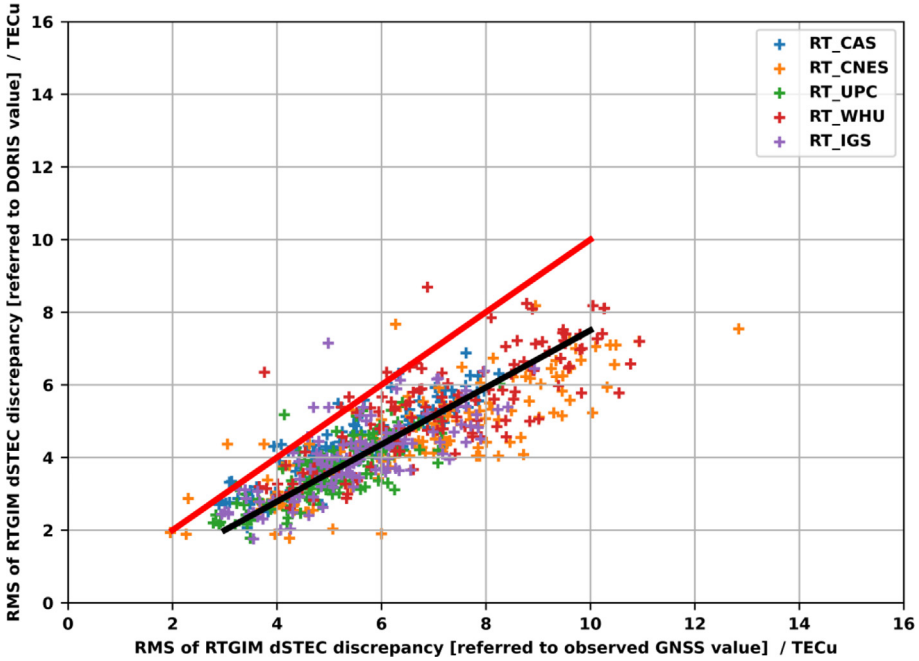

Fig. 9. RMS of RT-GIM dSTEC discrepancy referring to DORIS data versus that referring to GPS/GLONASS data during DOY 001–110, 2022. Red and black lines represent the symmetry and fitted lines, respectively.

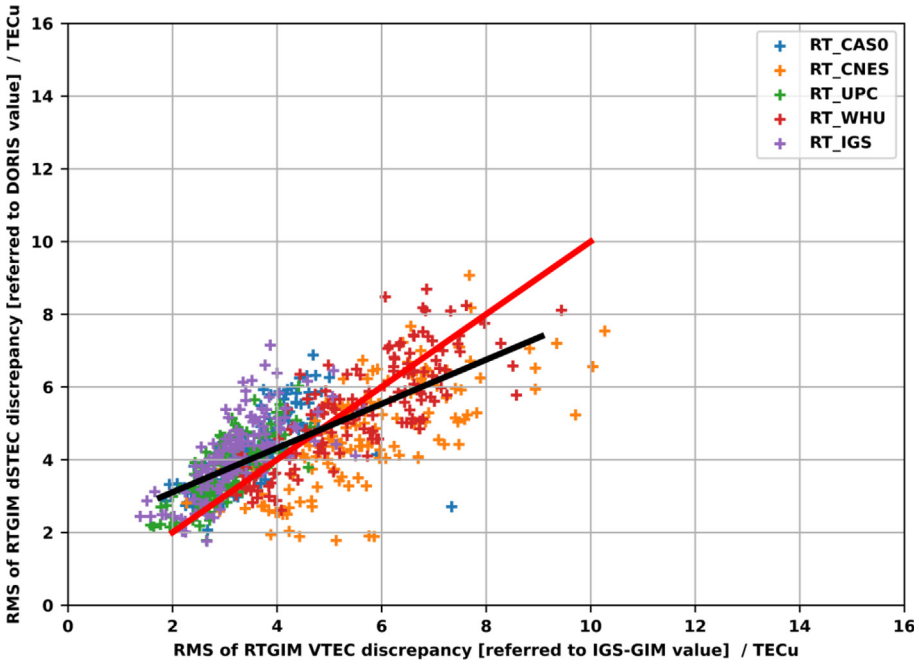

Fig. 10. RMS of RT-GIM dSTEC discrepancy referring to DORIS data versus that RMS of VTEC discrepancy referring to IGS-GIM during DOY 001–110, 2022. Red and black lines represent the symmetry and fitted lines, respectively.

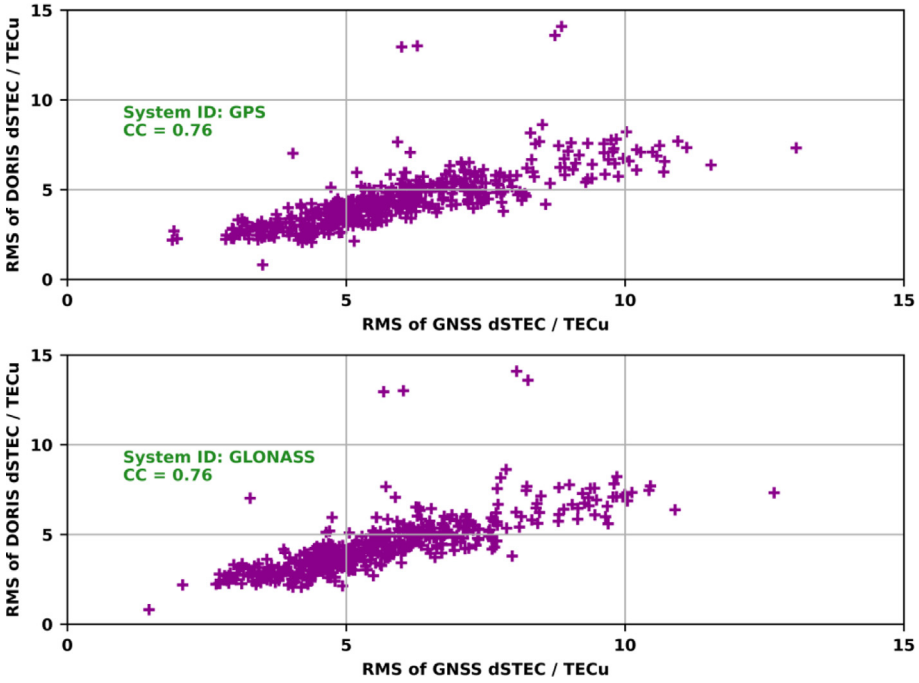

Fig. 11. Correlations between the RMS of DORIS dSTEC analysis and that of GPS dSTEC analysis (top), as well as the RMS of DORIS dSTEC analysis and that of GLONASS dSTEC analysis (bottom).

and GLONASS-only dSTEC assessments. As shown in Fig. 11, the Pearson correlation coefficients are identical (i.e., 0.76) in GPS-only and GLONASS-only dSTEC analysis, which indicates no significant dependence on the GNSS data used. However, such assumption requires further verification with the use of Galileo and BeiDou observations in future analysis.

DORIS and GNSS dSTEC analysis results are divided into six groups according to the satellite elevation angles, i.e. [15°, 25°], [25°, 35°], [35°, 45°], [45°, 55°], [55°, 65°] and [65°, 90°], respectively. The daily RMS of all IAACs' RT-GIMs in comparison to DORIS and GNSS dSTECs are calculated, to check the consistency of DORIS and GNSS assessments with respect to the variation of satellite

elevations. As shown in Fig. 12, large DORIS/GNSS dSTEC RMS is found for the group of low satellite elevations, and small RMS is observed for the group of high satellite elevations (see x- and y-axis). For DORIS dSTEC validation, the RMS drops from 9 TECu of low elevation group to only 2 TECu of high elevation group. For GNSS dSTEC validation, the RMS decreases from 15 TECu to around 3 TECu. Since dSTEC information is calculated as the difference between a given STEC and the STEC at the highest elevation angle, the dSTEC differences of low satellite elevations should suffer from large ionospheric mapping errors (i.e., model derived dSTEC) and observation noises (i.e., DORIS or GNSS derived dSTEC). As such, large RMS results can be expected for those of low satellite elevations. We also analyze the standard deviation between DORIS and GNSS dSTEC validations, to check the degree of dispersion of DORIS and GNSS analysis results. For each individual group of satellite elevations, the resulting STD value is 1.83, 1.52, 1.41, 0.59, 0.43 and 0.36 TECu, respectively. Note that the STD significantly drops below 0.59 TECu for the satellite elevation higher than 45°. It indicates that the dSTEC analysis with a high satellite elevation cutoff angle, e.g., 45°, can ensure a good consistency between DORIS and GNSS dSTEC assessments.

5. Summary and conclusions

The quality assessment of ground GNSS generated ionospheric electron content models is presently still an open question. In addition to altimetry VTEC information over the oceanic regions, limited external data sources are available today to perform a fully independent validation of those ionospheric models. DORIS data provides a valuable opportunity to study the ionosphere, given its homogeneous distribution of global beacon network and large relative frequency ratio between its two frequencies. The standardization of DORIS data formats as well as the decreasing time latency in obtaining DORIS observations, also makes it possible to analyze the model performance in near-real-time. In this paper, the DORIS-dSTEC concept is proposed for the independent performance assessment of GNSS-derived ionospheric models. As a first step, NRT DORIS data from Jason-3 satellite was used to evaluate the quality of RT-GIMs from different analysis centers of the IGS.

The concept of DORIS dSTEC assessment is presented, which is the extension of the existing GNSS dSTEC validation method. DORIS dSTEC can be directly calculated from the dual-frequency DORIS carrier measurements of modern DORIS receivers. Benefitting from the large rela-

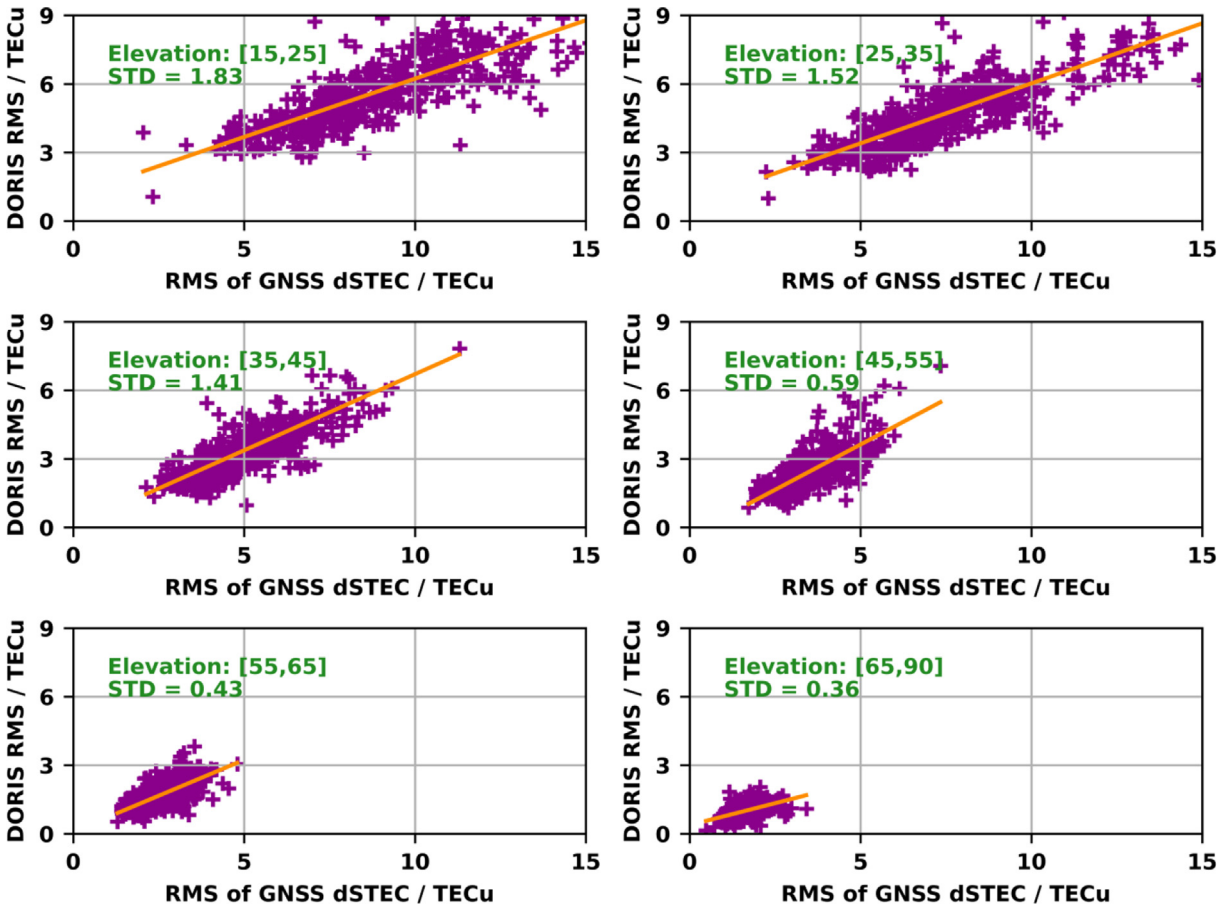

Fig. 12. Comparison between DORIS and GNSS dSTEC assessments within individual groups of satellite elevations.

tive frequency ratio between DORIS L1 (2 GHz) and L2 (400 MHz) frequencies, the theoretical precision of DORIS derived dSTEC reaches 0.028 TECu, which is around 10 times better than that of GNSS L1/L2 based dSTEC. Based on a global network of 48 DORIS beacon sites and co-located IGS stations, performance of the present 5 RT-GIMs from CAS, CNES, UPC, WHU as well as the IGS RT-combined one is evaluated in both DORIS and GNSS dSTEC validations. Using more than 18,000,000 DORIS dSTEC observables, the bias and STD is found to be 0.14 and 4.38 TECu between RT-GIM derived dSTEC and DORIS observed dSTEC and no systematical bias is found. The latitudinal variation and hemispheric asymmetry of RT-GIM errors, which have been well recognized in previous GPS-dSTEC or altimetry-VTEC validations, can also be clearly observed in DORIS dSTEC assessment. RMS of RT-GIM errors generated in DORIS dSTEC analysis is in general smaller than that referring to GNSS dSTEC. In both DORIS and GNSS dSTEC assessments, RT-GIMs from CNES and WHU show notably worse performance than the other three RT-GIMs. The overall Pearson correlation coefficient reaches 0.81 for the validation result using DORIS and GNSS dSTEC. To ensure a better consistency between DORIS and GNSS dSTEC assessments, the dSTEC analysis is suggested to be performed with the higher satellite elevation cutoff angle, e.g., 45°. The result confirms that DORIS dSTEC assessment can be used an independent way to validate the quality of those ground GPS/GNSS generated ionospheric models.

This study only uses co-located DORIS/GNSS stations in order to ensure a fair comparison between DORIS and GNSS dSTEC validation. However, for future validation activities, all DORIS beacons can and should be used. This will lead to a more homogeneous data distribution covering also more ocean areas. The DORIS NRT measurements are fully independent to GNSS derived ionospheric observables, which provides an independent way for the performance analysis of GNSS-generated ionospheric models, e.g., the RT-GIM analyzed in this work. In addition to Jason-3, more satellite missions providing NRT DORIS data are planned, which will indeed extend the coverage of DORIS ionospheric observables and benefit the ionospheric associated analysis. In the next step, we will continue the work on the analysis of dSTEC consistency between DORIS and those new GNSS constellations, e.g., BDS and Galileo. The feasibility of using DORIS data in the generation of real-time global ionospheric maps will also be analyzed.

Declaration of Competing Interest

The authors declare that they have no known competing financial interests or personal relationships that could have appeared to influence the work reported in this paper.

Acknowledgments

The authors acknowledge the International DORIS Service (IDS), International GNSS Service (IGS) and CAS Ionosphere Associate Analysis Center for providing GNSS data, DORIS data and RT-GIMs. This work was supported by the National Key R&D Program of China (2021YFB3901300), National Natural Science Foundation of China (42074043, 42122026, 42174038), Alliance of International Science Organizations (ANSO-CR-KP-2020-12), Youth Innovation Promotion Association and Future Star Program of the Chinese Academy of Sciences.

References

Auriol, A., Tourain, C., 2010. DORIS system: the new age. Adv. Space Res. 46 (12), 1484–1496. https://doi.org/10.1016/j.asr.2010.05.015.

Azpilicueta, F., Brunini, C., 2009. Analysis of the bias between TOPEX and GPS vTEC determinations. J. Geod. 83 (2), 121–127. https://doi.org/10.1007/s00190-008-0244-7.

Dettmering, D., Limberger, M., Schmidt, M., 2014. Using DORIS measurements for modeling the vertical total electron content of the Earth's ionosphere. J. Geod. 88 (12), 1131–1143. https://doi.org/10.1007/s00190-014-0748-2.

Erdogan, E., Schmidt, M., Goss, A., Görres, B., Seitz, F., 2020. Adaptive modeling of the global ionosphere vertical total electron content. Remote Sens. (Basel) 12 (11), 1822. https://doi.org/10.3390/rs12111822.

Erdogan, E., Schmidt, M., Goss, A., Görres, B., Seitz, F., 2021. Real-time monitoring of ionosphere VTEC using Multi-GNSS carrier-phase observations and B-splines. Space Weather 19 (10). https://doi.org/10.1029/2021sw002858.

Fleury, R., Foucher, F., Lassudrie-Duchesne, P., 1991. Global TEC measurement capabilities of the DORIS system. Adv. Space Res. 11 (10), 51–54. https://doi.org/10.1016/0273-1177(91)90321-A.

Goss, A., Hernández-Pajares, M., Schmidt, M., Roma-Dollase, D., Erdogan, E., Seitz, F., 2020a. High-Resolution ionosphere corrections for single-frequency positioning. Remote Sens. (Basel) 13 (1), 12. https://doi.org/10.3390/rs13010012.

Goss, A., Schmidt, M., Erdogan, E., Seitz, F., 2020b. Global and regional high-resolution VTEC modelling using a two-step B-Spline approach. Remote Sens. (Basel) 12 (7), 1198. https://doi.org/10.3390/rs12071198.

Hernández-Pajares, M., Juan, J.M., Sanz, J., Orus, R., Garcia-Rigo, A., Feltens, J., Krankowski, A., 2009. The IGS VTEC maps: a reliable source of ionospheric information since 1998. J. Geod. 83 (3–4), 263–275. https://doi.org/10.1007/s00190-008-0266-1.

Hernández-Pajares, M., Roma-Dollase, D., Krankowski, A., García-Rigo, A., Orús-Pérez, R., 2017. Methodology and consistency of slant and vertical assessments for ionospheric electron content models. J. Geod. 91 (12), 1405–1414. https://doi.org/10.1007/s00190-017-1032-z.

Hernández-Pajares, M., Lyu, H., Garcia-Fernandez, M., Orus-Perez, R., 2020. A new way of improving global ionospheric maps by ionospheric tomography: consistent combination of multi-GNSS and multi-space geodetic dual-frequency measurements gathered from vessel-, LEO- and ground-based receivers. J. Geod. 94 (8), 1–16. https://doi.org/10.1007/s00190-020-01397-1.

IDS, 2006. RINEX DORIS 3.0. Accessible from https://ids-doris.org/documents/BC/data/RINEX_DORIS.pdf. [Accessed 18 November 2022].

IDS, 2021. DORIS satellites models implemented in POE processing. Accessible from https://ftp.ids-doris.org/pub/ids/satellites/DORISSatelliteModels.pdf. [Accessed 18 November 2022].

IGS, 2020. IGS State Space Representation (SSR) Format Version 1.00, International GNSS Service (IGS). Accessible from https://files.igs.org/pub/data/format/igs_ssr_v1.pdf. [Accessed 18 November 2022].

Li, Z., Wang, N., Hernández-Pajares, M., Yuan, Y., Krankowski, A., Liu, A., Blot, A., 2020. IGS real-time service for global ionospheric total electron content modeling. J. Geod. 94 (3), 1–16. https://doi.org/10.1007/s00190-020-01360-0.

Li, Z., Yuan, Y., Wang, N., Hernandez-Pajares, M., Huo, X., 2015. SHPTS: towards a new method for generating precise global ionospheric TEC map based on spherical harmonic and generalized trigonometric series functions. Journal of Geodesy 89 (4), 331–345 https://doi.org/10.1007/s00190-014-0778-9.

Liu, Q., Hernández-Pajares, M., Yang, H., Monte-Moreno, E., Roma-Dollase, D., García-Rigo, A., Ghoddousi-Fard, R., 2021. The cooperative IGS RT-GIMs: a reliable estimation of the global ionospheric electron content distribution in real time. Earth Syst. Sci. Data 13 (9), 4567–4582. https://doi.org/10.5194/essd-13-4567-2021.

Liu, A., Wang, N., Li, Z., Zhou, K., Yuan, H., 2018. Validation of CAS's final global ionospheric maps during different geomagnetic activities from 2015 to 2017. Results Phys. 10, 481–486. https://doi.org/10.1016/j.rinp.2018.06.057.

Liu, A., Li, Z., Wang, N., Zhang, Y., Krankowski, A., Yuan, H., 2023. SHAKING: Adjusted spherical harmonics adding KrigING method for near real-time ionospheric modeling with multi-GNSS observations. Advances in Space Research 71 (1), 67–79 https://doi.org/10.1016/j.asr.2022.07.049.

Liu, A., Wang, N., Li, Z., Wang, Z., Yuan, H., 2019. Assessment of NeQuick and IRI-2016 models during different geomagnetic activities in global scale: Comparison with GPS-TEC, dSTEC, Jason-TEC and GIM. Adv. Space Res. 63 (12), 3978–3992. https://doi.org/10.1016/j.asr.2019.02.032.

Lyu, H., Hernández-Pajares, M., Nohutcu, M., García-Rigo, A., Zhang, H., Liu, J., 2018. The Barcelona ionospheric mapping function (BIMF) and its application to northern mid-latitudes. GPS Solutions 22 (3), 67. https://doi.org/10.1007/s10291-018-0731-0.

Mercier, F., Cerri, L., Berthias, J.-P., 2010. Jason-2 DORIS phase measurement processing. Adv. Space Res. 45 (12), 1441–1454. https://doi.org/10.1016/j.asr.2009.12.002.

Ren, X., Chen, J., Li, X., Zhang, X., Freeshah, M., 2019. Performance evaluation of real-time global ionospheric maps provided by different IGS analysis centers. GPS Solutions 23 (4), 1–17. https://doi.org/10.1007/s10291-019-0904-5.

Roma-Dollase, D., Hernández-Pajares, M., Krankowski, A., Kotulak, K., Ghoddousi-Fard, R., Yuan, Y., Gómez-Cama, J.M., 2017. Consistency of seven different GNSS global ionospheric mapping techniques during one solar cycle. J. Geod. 92 (6), 691–706. https://doi.org/10.1007/s00190-017-1088-9.

RTCM-SC, 2016. RTCM Standard 10403.3 Differential GNSS (Global Navigation Satellite System) Services—Version 3, RTCM Special Committee 104. Accessible from https://www.rtcm.org. [Accessed 18 November 2022].

Schaer, S., Gurtner, W. and Feltens, J., 1998. IONEX: The ionosphere map exchange format version 1. Proceedings of the IGS AC workshop, Darmstadt, Germany. Accessible from https://files.igs.org/pub/data/format/ionex1.pdf. [Accessed 18 November 2022].

Wang, N., Li, Z., 2018. Consistency of DORIS and GPS Assessments for the Real-time Global Ionospheric Maps. Presented at the IDS Workshop, Ponta Delgada, São Miguel Island, Azores Archipelago. https://ids-doris.org/images/documents/report/ids_workshop_2018/IDS18_s4_Ningbo_ConsistencyDORISandGPSforRTionoMaps.pdf. [Accessed 18 November 2022].

Wang, N., Yuan, Y., Li, Z., Li, Y., Huo, X., Li, M., 2016. An examination of the Galileo NeQuick model: comparison with GPS and JASON TEC. GPS Solutions 21 (2), 605–615. https://doi.org/10.1007/s10291-016-0553-x.

Wang, N., Li, Z., Yuan, Y., Huo, X., 2021. BeiDou Global Ionospheric delay correction Model (BDGIM): performance analysis during different levels of solar conditions. GPS Solutions 25 (3), 1–13. https://doi.org/10.1007/s10291-021-01125-y.

Willis, P., Soudarin, L., Jayles, C., Rolland, L., 2007. DORIS applications for solid earth and atmospheric sciences. C. R. Geosci. 339 (16), 949–959. https://doi.org/10.1016/j.crte.2007.09.015.

Yang, H., Monte-Moreno, E., Hernández-Pajares, M., Roma-Dollase, D., 2021. Real-time interpolation of global ionospheric maps by means of sparse representation. J. Geod. 95 (6), 1–20. https://doi.org/10.1007/s00190-021-01525-5.

Zhang, Q., Zhao, Q., 2018. Global ionosphere mapping and differential code bias estimation during low and high solar activity periods with GIMAS software. Remote Sens. (Basel) 10 (5), 705. https://doi.org/10.3390/rs10050705.